

Crystal Structure of Thecotrichite, an Efflorescent Salt on Calcareous Objects Stored in Wooden Cabinets

Nanna Wahlberg,[†] Tomče Runčevski,[‡] Robert E. Dinnebier,^{*,‡} Andrea Fischer,[§] Gerhard Eggert,[§] and Bo B. Iversen[†]

[†]Department of Chemistry and iNANO, Center for Materials Crystallography, Langelandsgade 140, Aarhus C 8000, Denmark

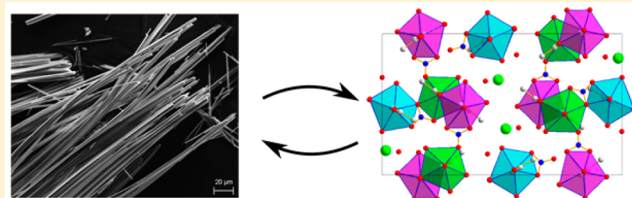
[‡]Max-Planck-Institute for Solid State Research, Heisenbergstrasse 1, 70569 Stuttgart, Germany

[§]State Academy of Art and Design Stuttgart, Am Weißenhof 1, 70191 Stuttgart, Germany

S Supporting Information

ABSTRACT: The crystal structure of thecotrichite, $\text{Ca}_3(\text{CH}_3\text{COO})_3\text{Cl}(\text{NO}_3)_2 \cdot 6\text{H}_2\text{O}$, an efflorescent salt occurring on surfaces of porous calcareous objects stored in wooden cabinets, was solved *ab initio* from high-resolution, laboratory X-ray powder diffraction data. The compound was found to contain one water molecule per formula unit less than what was previously reported. The crystal structure of thecotrichite ($P2_1/a$, $Z = 4$, $a = 23.5933(4)$, $b = 13.8459(3)$, $c = 6.8010(1)$

\AA , $\beta = 95.195(2)^\circ$, $V = 2212.57(7) \text{\AA}^3$) consists of a network of calcium ions, connected through acetate and nitrate ions, forming a metal–organic framework. In addition, five of the six chemically different water molecules are directly coordinated to the calcium ions, with the remaining water molecule located in the interstitial space, together with the chloride ion. The needle-like morphology of the microcrystals was rationalized from the crystal structure. It is suggested that the crystallite growth mechanism depends heavily on the porous nature of the crystal structure. The thermal characteristics and stability of the material were studied. Structural and spectroscopic information on this efflorescent salt are provided to ease its characterization and identification, especially in museums and art collections worldwide.



INTRODUCTION

The formation of efflorescent salts onto surfaces of porous calcareous objects has been a problem known for over a century. The efflorescence on shells, later called Byne's disease, was first reported in 1896.^{1,2} Thirty years later, it was found that acetic acid is the main contributor to the surface damage.³ Considerable amounts of acetic acid vapor are emitted from wood (especially oak), used to make storage cabinets and display cases. During the pioneering research on this degradation process, two compounds were found to be among the major products: calclacite, $\text{Ca}(\text{CH}_3\text{COO})\text{Cl} \cdot \text{SH}_2\text{O}$, whose crystal structure was reported,⁴ and “efflorescence X”, whose exact composition and structure have remained ambiguous ever since.⁵ Efflorescence X was later renamed as thecotrichite and became one of the most frequently observed efflorescent salts on rare ceramic and limestone objects in museums (one example is given in Figure 1a,b).^{4,6,7} Gibson et al., using a combination of powder diffraction, ion chromatography, infrared spectroscopy, NMR, and thermogravimetry, reported the cotrichite's composition to be $\text{Ca}_{2.95}(\text{CH}_3\text{COO})_{2.91}\text{Cl}_{0.97}(\text{NO}_3)_{2.03} \cdot 6.55\text{H}_2\text{O}$.⁸ The chemical formula was simplified to $\text{Ca}_3(\text{CH}_3\text{COO})_3\text{Cl}(\text{NO}_3)_2 \cdot 7\text{H}_2\text{O}$, and the actual amount of water in the structure remained uncertain. Crystal structure determination of this important efflorescent salt failed, presumably due to the unavailability of single crystals of quality suitable for single crystal diffraction

(thecotrichite crystallizes in the form of microcrystalline needles, as shown in Figure 1c,d). However, the microcrystallinity presents no obstacle for powder X-ray diffraction (PXRD), and after careful grinding thecotrichite becomes amenable to structural investigations.

The limited structural knowledge on thecotrichite has severely hindered its identification and characterization. Visually, it is very difficult to discriminate it from other calcium acetates (and calcites), as neither its white color nor needle-like morphology is unique. Its powder diffraction signature was only communicated, but without any report on the crystal structure.^{8,9} Identification by spectroscopic methods is challenging and ambiguous (as these efflorescent salts sometimes occur in mixtures and they might have similar spectra).⁸ Traditionally, the presence of thecotrichite on affected surfaces has been only speculated, based on visual inspection and on knowledge of the storage history of the suffered object. Herein, we present the PXRD pattern, detailed crystal structure solution and Rietveld refinement, and the results of Raman spectroscopic investigations and thermal analyses (TG and DTA) performed on this frequently observed efflorescent salt. PXRD can easily identify and quantify crystalline phases with

Received: February 9, 2015

Revised: April 29, 2015

Published: May 6, 2015



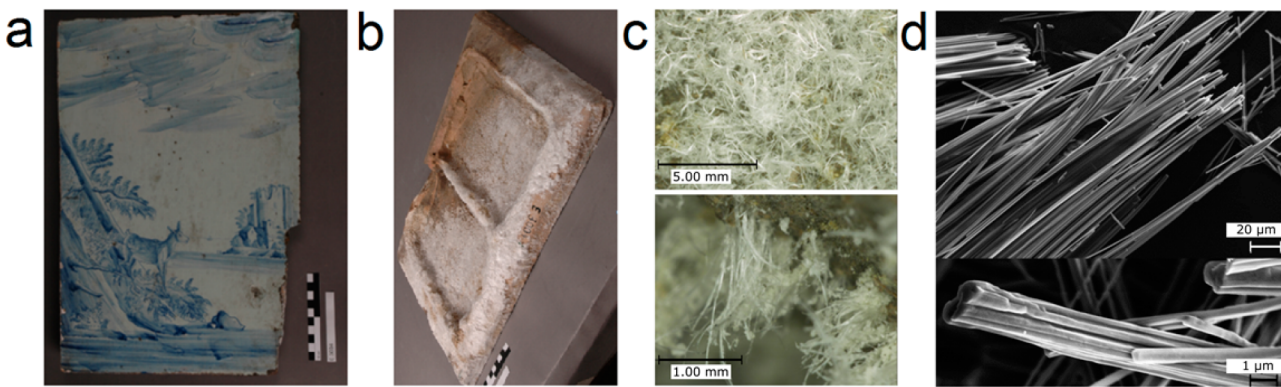


Figure 1. Thecotrichite on a glazed tile from the collection of Landesmuseum Württemberg (a) and its backside (b) covered with white thecotrichite crystals in (c). (d) FE-SEM images of the thecotrichite microcrystals.

known crystal structures.^{10,11} Raman spectroscopy is particular useful as a nondestructive *in operando* detection technique, including surface reactions studies.^{12–14} The information presented in this article aid the identification and characterization of thecotrichite on affected objects by PXRD and Raman spectroscopy, which are easily executable even by nonspecialized chemists.

EXPERIMENTAL SECTION

Sample. The sample of thecotrichite was obtained from the surface of a glazed ceramic tile, dating to early modern times, manufactured in Southern Germany, with size of $41 \times 29 \times 3.5$ cm, and part of the collection of Landesmuseum Württemberg, no. E 3004. The tile was stored from the 1980s until 2004 in wooden cupboards. The backside heavily suffered thecotrichite efflorescence occurring as a phase-pure product (Figure 1).

Powder X-ray Diffraction and Crystal Structure Solution and Refinement. PXRD data (Figures 2 and 4b) were collected on a high-

covering the range $5\text{--}60^\circ$ in 2θ with a step size of 0.015° . PXRD data were collected in the temperature range from $30\text{ }^\circ\text{C}$ up to $210\text{ }^\circ\text{C}$ with $20\text{ }^\circ\text{C}$ intervals, using a hot air blower for heating the sample.

Indexing, structure solution, and Rietveld refinement were performed with the TOPAS 4.2 program suite.¹⁵ The iterative least-squares algorithm (LSI)¹⁶ was employed to index the pattern and resulted in a primitive monoclinic lattice (see Table 1 for unit cell

Table 1. Selected Crystallographic and Structural Details on $\text{Ca}_3(\text{CH}_3\text{COO})_3\text{Cl}(\text{NO}_3)_2\cdot6\text{H}_2\text{O}$

formula	$\text{Ca}_3(\text{CH}_3\text{COO})_3\text{Cl}(\text{NO}_3)_2\cdot6\text{H}_2\text{O}$
crystal system	monoclinic
space group	$P2_1/a$
Z	4
a [Å]	23.5933(4)
b [Å]	13.8459(3)
c [Å]	6.8010(1)
β [$^\circ$]	95.195(2)
V [Å 3]	2212.57(7)
T [K]	303
wavelength [Å]	1.54059
$R\text{-exp}$ [%]	1.595
$R\text{-p}$ [%]	3.581
$R\text{-wp}$ [%]	4.743
$R\text{-Bragg}$ [%]	3.226
2θ range [$^\circ$]	5.5 to 59
step width [$^\circ$]	0.015
time/scan [h]	6
no. of variables	112

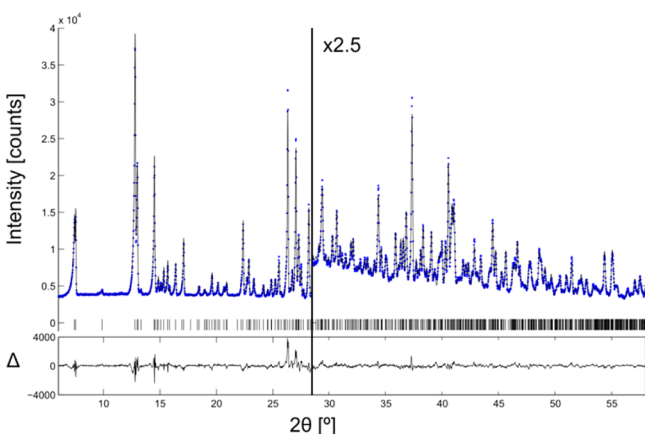


Figure 2. Scattered X-ray intensities of thecotrichite at ambient conditions, as a function of diffraction angle. The observed pattern (diamonds) measured in Debye–Scherrer geometry, the best Rietveld fit profiles (line), and the difference curve between the observed and the calculated profiles (below) are shown. The high angle part is enlarged for clarity.

resolution Stoe Stadi-P laboratory powder diffractometer in Debye–Scherrer geometry. The diffractometer was equipped with a Cu-source, where the selected $\text{Cu-K}\alpha_1$ radiation was obtained by a Johann-type Ge monochromator. A linear position sensitive silicon-strip detector (Mythen-Dectris) was used, with an opening angle of approximately 13° . The patterns were collected on a rotated sample (for better particle statistics) packed in a glass capillary, for a period of 6 h

parameters). The most probable space group was found to be $P2_1/a$ based on the observed reflection extinctions. The unit cell and profile parameters were refined by a Pawley fit,¹⁷ using the fundamental parameters approach.¹⁸ The background was modeled by a Chebychev polynomial of 8th order and a $1/X$ function, mainly describing the air scattering at low diffraction angles.

The positions of the Ca atoms and most of the coordinating oxygen atoms were readily determined by applying the charge flipping algorithm¹⁹ supported by inclusion of the tangent formula.²⁰ The rest of the atoms were located by combining the global optimization method of simulated annealing (SA)²¹ and inspection of difference Fourier maps ($F_{\text{obs}} - F_{\text{calc}}$). The crystal structure was refined using the Rietveld whole-pattern refinement method.²² The atomic positions were refined employing restraints (based on ideal bond lengths and angles for the acetic acid and nitrate groups). The hydrogen atom positions were calculated by Mercury.²³ An overall atomic displacement parameter for the atoms was refined. The apparent anisotropic peak broadening due to microstrain was modeled by including

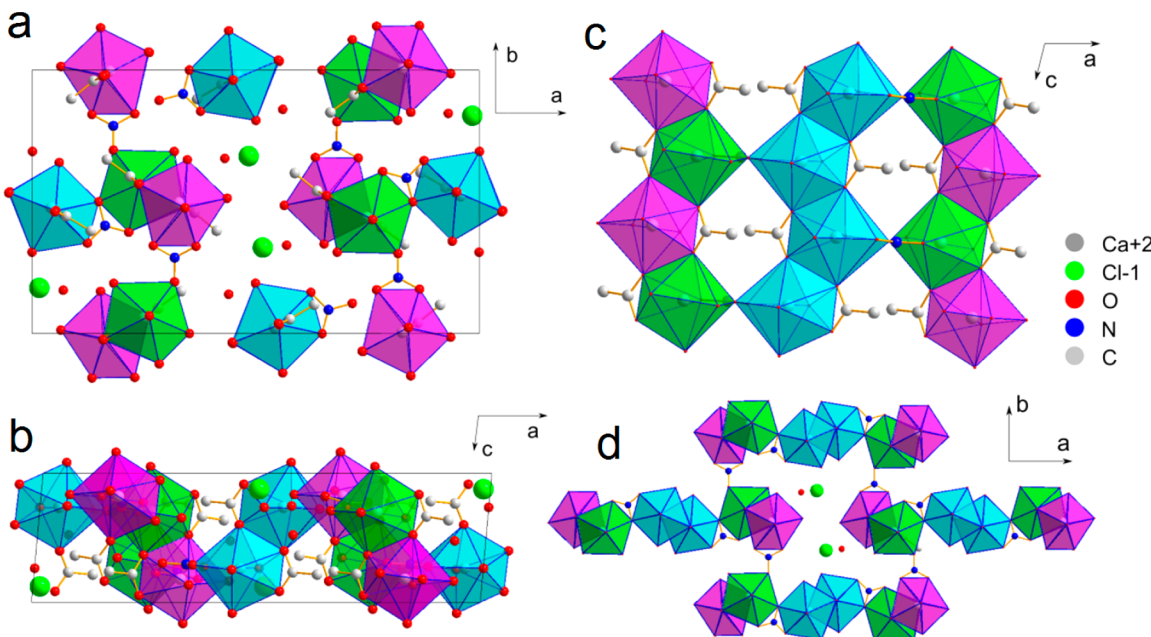


Figure 3. Crystal structure and unit cell content of thecotrichite, presented (a) along the *c*-axis and (b) along the *b*-axis. Extended crystal packing motif of thecotrichite viewed (c) along the *b*-axis and (d) along the *c*-axis. Polyhedra colors: Ca1: magenta, Ca2: cyan, Ca3: green.

spherical harmonics of the second order. The crystal structure and further crystallographic information is available in the crystallographic information file (CIF), deposit number: CCDC 1043649.

Differential Thermal Analysis. Thermal analysis was conducted on a Netzsch STA 409 C instrument. The sample (2.9965 mg) was heated from 27.5 °C up to 800 °C with a heating rate of 5 °C/min in an atmosphere of ambient air (flow rate 1 mL/min).

Raman Spectroscopy. Micro-Raman spectra were recorded by using a Renishaw inVia Raman spectrometer (grating 1800 L/mm, resolution 1 cm⁻¹) equipped with a Leica DMLM microscope and a RenCam CCD detector. The spectra were taken from 100 to 3700 cm⁻¹, using a He–Ne laser operating at 632.8 nm. The power of the laser was less than 900 μW focused into a 0.7 μm spot through a 50× microscope objective.

Scanning Electron Microscopy. FE-SEM images were obtained using a Zeiss SUPRA 40 VP microscope (acceleration voltages of 5 and 10 kV, SE detector).

RESULTS AND DISCUSSION

Crystal Structure Description. The crystal structure of thecotrichite was *ab initio* solved and refined directly from the laboratory PXRD data. The unit cell content and the crystal packing are presented in Figure 3. Three crystallographically different CaO₈ polyhedra are identified and drawn in Figure 3 in different colors (Ca1: magenta, Ca2: cyan, Ca3: green). Most of the coordinating oxygen atoms (six oxygen atoms to Ca1 and Ca2, and seven to Ca3) are donated by either acetate or nitrate ions. The remaining one (for Ca3) and two (for Ca1 and Ca2) coordinating oxygen atoms belong to the water molecules. Therefore, five out of six water molecules per formula unit are directly coordinated to the calcium cations, with the remaining water molecule placed in the interstitial position. The interstitial space also hosts the chloride anion. The polyhedra around Ca1 and Ca3 are edge sharing and are repeated in an alternating fashion along the crystallographic *c*-axis. The resulting chain-like structure is shown in Figure 3c. The polyhedra around Ca2 by themselves form a similar chain-like arrangement running along the crystallographic *c*-axis. All calcium polyhedra are bridged by an acetate ion, with both

oxygen atoms coordinating two neighboring calcium ions. The chain-like structure of the acetate bridged calcium polyhedra is also observed in the related calcareous efflorescent salt, the calclacite.⁴ Independent chains of Ca polyhedra are linked to each other via corner sharing (Ca2 to Ca3), and they are bridged by the nitrate anions. Therefore, they build triple chains (one is presented in Figure 3c). The triple chains are further connected to their neighbors via nitrate anions, forming covalently bonded layers of well-separated polyhedra, resting on the *a*–*b* plane (intersect of four interconnected triple chains is presented in Figure 3d).

The resulting metal–organic framework (MOF) has channels running along the *c*-axis, which are occupied by chloride ions and uncoordinated water molecules (Figure 3d). The interstitial water molecules are bonded to the coordinated water molecules via hydrogen bonding (with O–O distances of 2.850, 2.892, and 2.979 Å) and to the chloride anion (with an O–Cl distance of 3.107 Å), thus forming a hydrogen bonded network of medium strength. It should be mentioned that the hydrogen bonding network might strongly influence the crystal size and shape.²⁴ Additionally, the chloride anion is bonded to three other neighboring water molecules of the Ca polyhedra (with O–Cl distances of 3.126, 3.100, and 3.195 Å).

High Temperature Behavior. It has been reported that the first thermally induced process of thecotrichite is partial dehydration from 60 to 120 °C.⁸ In fact, the porous nature of the crystal structure promises dehydration at mild temperatures by removal of the uncoordinated water molecules resting in the channels. During this possible dehydration process, the framework structure and electroneutrality would remain intact. To test this assumption and to reinvestigate the thermal behavior of thecotrichite, thermal analyses (TG and DTA) and *in situ* variable temperature PXRD measurements were performed (Figure 4).

TG data were collected up to 300 °C (Figure 4a), revealing three mass-loss steps in the 30–250 °C temperature window. Heating the sample to 150 °C results in a continuous mass reduction, which eventually reaches 1.3% and accounts for

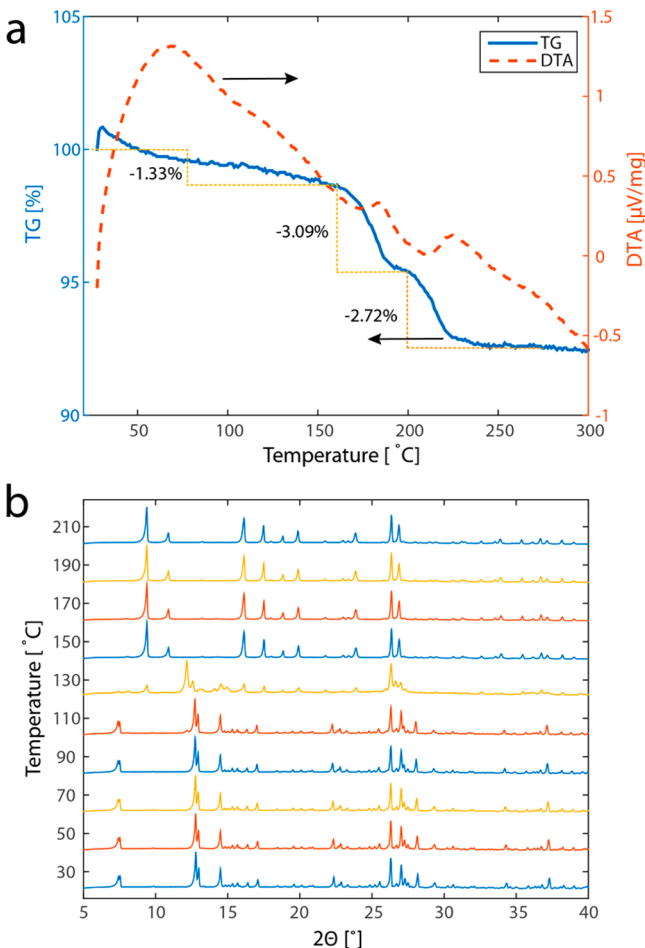


Figure 4. (a) Thermogravimetric (TG) scan of thecotrichite (scan rate 5 °C/min). (b) XRPD data of thecotrichite in the temperature range 30–210 °C.

almost half a water molecule per formula unit. In this thermal region, the DTA curve shows a featureless slope, which is a further indication of structural stability in the given temperature range. The *in situ* collected multitemperature PXRD patterns confirm that within this temperature interval thecotrichite retains its crystal structure (Figure 4b). Precise unit cell parameters at elevated temperatures were determined by Pawley fitting and are listed in Table 2. With increasing the temperature, the unit cell exhibits anisotropic thermal expansion: The *a*- and *b*-axes expand, whereas the *c*-axis shows near-to-zero expansion. This observation is in accordance with the features of the crystal structure: along the *c*-axis the Ca polyhedra are densely packed (with edge sharing), whereas in the *a*–*b* plane the metal cations network is either corner-shared or bridged by nitrate anions. The accumulated strength of the bonds along the chains is higher

and, therefore more heat resistant, than in any of the other directions.

The *in situ* XRPD patterns collected at temperatures higher than 110 °C (Figure 4b) show a structural decomposition of thecotrichite and formation of a new lower hydrated phase. This thermal decomposition is also detected in the TG curve (Figure 4a): Between 150 and 200 °C, a mass reduction of 3.0% is observed (ca. one water molecule per formula unit). The DTA curve confirms the process with a corresponding maximum in the curve. The onset of decomposition is observed at higher temperatures in the thermal analyses than in the diffraction measurements, and this discrepancy probably originates from differences in the experimental conditions (predominantly heating rates). The phase formed above 110 °C is not stable at high temperatures and readily decomposes on further heating, as observed with a second well-defined mass-loss step in TG curve in the range from 200 to 250 °C with a 2.7% loss of mass (ca. one water molecule per formula unit). This thermal decomposition is also evidenced by a peak maximum in the DTA curve (Figure 4b). In the previous report on the thermal stability of thecotrichite, these two steps were reported as a single mass-loss process,⁸ presumably due to lower resolution of the data.

Morphology and Crystal Growth. The name thecotrichite is derived from the needle-like or hairy morphology of the microcrystals (from Greek: θέκη = chest and triches = hair).⁶ The thecotrichite crystals grow as bundles of elongated, hair-like crystallites, half a micrometer in diameter (Figure 1d) and millimeters in length (Figure 1c). The needle-like morphology can be rationalized by the Bravais–Friedel and Donnay–Harker (BFDH) model as implemented in Mercury.^{20–22} This model assumes the growth rate in a given crystallographic direction to be inversely proportional to the spacing between the corresponding lattice planes.²² In the case of thecotrichite, this results in a needle-like crystal, elongated in the direction of the *c*-axis, as shown in Figure 5.

The needle-like morphology and the crystal growth can be related to the crystal structure characteristics. Thus, the *a*–*b* plane of the unit cell is parallel to the substrate, and the crystal grows in the direction of the *c*-axis, resembling the growth of a hair. This fits well with the finding that the interaction along the *c*-axis is stronger than in the other directions. The porosity of the structure can possibly explain the formation mechanism. It is reasonable to assume that the channels along the *c*-axis serve as a transportation route through the crystal, bringing calcium ions from the substrate to its surface. Since the acetate, chloride, and nitrate ions come as pollutants from the environment,⁶ a continuous crystal growth is ensured. This reaction takes place at a very slow pace, on time scales of months or years. Therefore, it is expectedly different from most of the reactions conducted in the laboratory. This might be a reason for the unavailability of large single crystals.

Table 2. Unit Cell Parameters of Thecotrichite from 30 to 110 °C

temperature [°C]	<i>a</i> [Å]	<i>b</i> [Å]	<i>c</i> [Å]	β [°]	<i>V</i> [Å ³]
30	23.5933(4)	13.8459(3)	6.8010(1)	95.195(2)	2212.57(7)
50	23.6269(5)	13.8624(3)	6.8018(1)	95.186(2)	2218.65(8)
70	23.6548(5)	13.8799(3)	6.8020(1)	95.183(2)	2224.14(8)
90	23.6724(6)	13.8987(3)	6.8015(1)	95.189(2)	2228.64(9)
110	23.6773(8)	13.9148(5)	6.8007(2)	95.180(3)	2231.4(1)

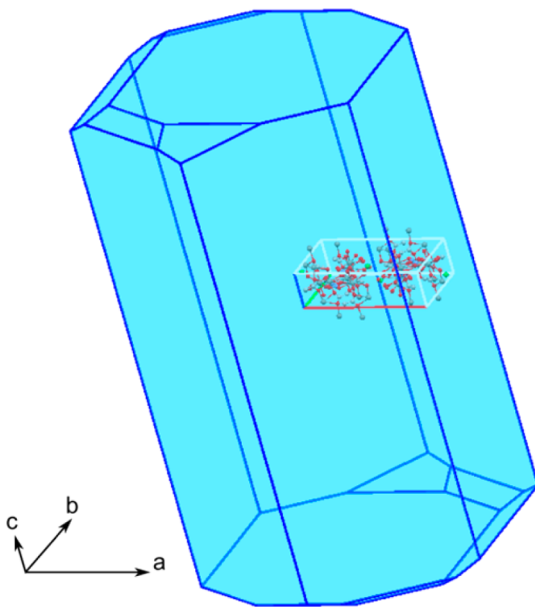


Figure 5. Simulation of the crystal morphology of thecotrichite based on the BFDH model.

Raman Spectroscopy. The Raman spectrum of thecotrichite is presented in Figure 6, together with assignment of the Raman bands, based on the spectra of other acetates, hydrates, and nitrates.^{29,30} It agrees with the spectrum presented on a poster at IRUG 7.³¹ It should be noted that the assignment of vibrations to certain Raman bands is tentative, and the accent of the study is put on the qualitative detection of the acetate and nitrate anions and on presenting the Raman spectrum (Figure 6c) as a fingerprint that can serve as easy identification of thecotrichite by Raman spectroscopy.

The low Raman shift part of the spectrum (Figure 6a), or the fingerprint region, is dominated by bands that can be ascribed to the acetate and nitrate groups. The low-frequency and low-intensity bands spreading from 600 to 800 cm⁻¹ might

originate from the COO deformation and rocking vibrations and the NO₃ bending vibrations. The characteristic C–C stretching vibration is observed as a doublet with peaks at 968 and 961 cm⁻¹. The acetate CH₃ rocking vibrations are observed at 1058 and 1046 cm⁻¹, probably together with a Raman band of the symmetry-reduced NO₃ symmetric stretching. The symmetric and asymmetric deformation vibrations of CH₃ contribute as low-intensity bands, positioned at 1431 and 1349 cm⁻¹.³² The characteristic NO₃ asymmetric stretching vibration is observed as a strong Raman peak centered at 1472 cm⁻¹.

The high Raman shift part of the spectrum (Figure 6b) is dominated by several Raman bands from the C–H stretching vibrations (from 2900 to 3050 cm⁻¹) and very low intensity bands from the O–H vibrations (centered at 3372 and 3470 cm⁻¹).

CONCLUSION

The crystal structure of thecotrichite, an efflorescence salt occurring on the surface of calcareous items (for example limestone and ceramics with lime deposits) in collections stored in wooden cabinets, was successfully solved, *ab initio* from high-resolution laboratory powder diffraction data, and refined by the Rietveld method. The present contribution concludes an over 100-year-old hunt to determine the exact chemical composition and the crystal structure of this frequently observed art efflorescent product. The exact chemical formula was found to be Ca₃(CH₃COO)₃Cl(NO₃)₂·6H₂O, correcting the report in the literature where this salt was presented as a heptahydrate.⁸ The crystal structure presents a metal–organic framework, constituted of calcium cations, 8-fold coordinated by oxygen atoms of the acetate and nitrate anions and water molecules. The calcium cations are arranged in a chain-like fashion, which propagate along the crystallographic *c*-axis. Their packing in the unit cell leaves open-ended channels, accommodating the chloride ions and part of the water molecules (one out of the six water molecules in the formula unit). The thecotrichite was proven to be thermally

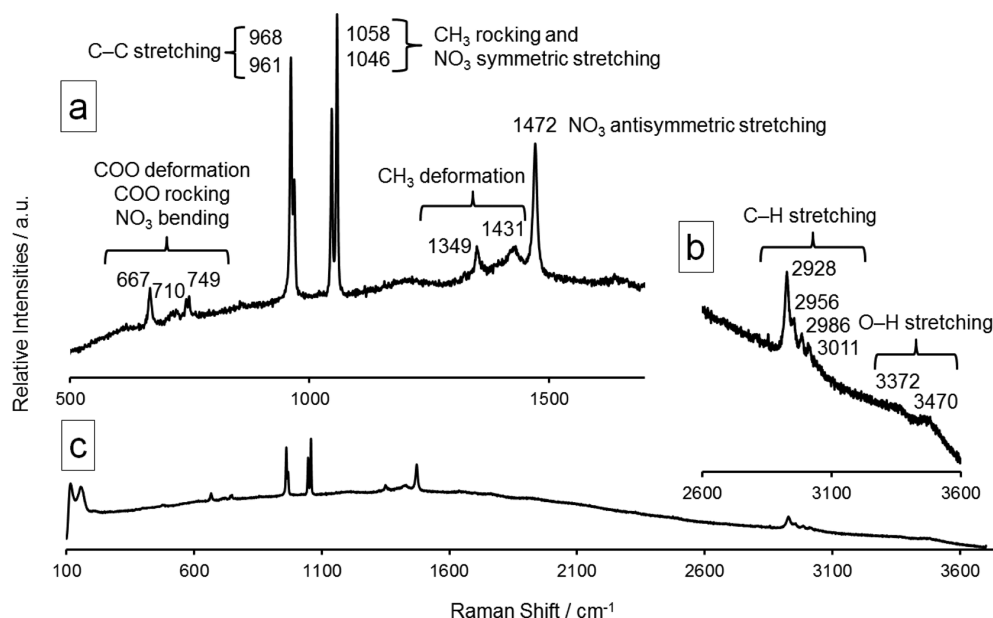


Figure 6. Raman spectroscopic analysis of thecotrichite. Tentative assignment of the low Raman shift region (a) and high Raman shift region (b). In (c) the complete recorded spectrum is shown.

stable when heated to temperatures lower than 130 °C. In this thermal range, part of the interstitial water molecules are continuously dehydrated; thus its hydration stage becomes slightly lower than hexahydrated. The maximum amount of water molecules that can be lost from the intact thecotrichite crystal structure is about half a water molecule per formula unit. At higher temperatures, two subsequent, thermally induced dehydration/decomposition processes take place. These processes cause further dehydration by two water molecules per formula unit, which leads to structural decomposition. The thecotrichite salt crystallizes in the form of elongated needle- or hair-like crystals. The formation mechanism of the crystallites was rationalized based on the channel-MOF crystal structure. It is suggested that Ca cations travel through the channels from the substrate to reach the outmost part of the crystal, which is rich in acetates, nitrates, and water from the atmosphere, and this ensures crystal growth. The Raman spectrum is presented and discussed to complement the structural analysis. Knowledge about the chemical composition and especially the crystal structure of thecotrichite is an important contribution that enables execution of qualitative and quantitative PXRD analyses of efflorescence on museum objects. Moreover, it helps to understand the deterioration processes in greater detail.

■ ASSOCIATED CONTENT

S Supporting Information

The crystallographic information file (CIF) is available online. The Supporting Information is available free of charge on the ACS Publications website at DOI: 10.1021/acs.cgd.5b00197.

■ AUTHOR INFORMATION

Corresponding Author

*E-mail: r.dinnebier@fkf.mpg.de.

Notes

The authors declare no competing financial interest.

■ ACKNOWLEDGMENTS

We would like to thank Daniel Weber (Max Planck Institute, Stuttgart) for the thermal analysis and Dirk Kirchner (German Mining Museum, Bochum) for taking the FE-SEM images. In addition, Marian Schüch and Rebekka Kuiter (State Academy of Art and Design Stuttgart) are acknowledged for the pictures of the efflorescence on the tile. The Danish National Research Foundation is thanked for support (DNRF93).

■ REFERENCES

- (1) Kenyon, A. F. *Pap. Proc. R. Soc. Tasmania* **1896**, 88.
- (2) Byne, L. S. G. *J. Conchol.* **1899**, 9, 172–178.
- (3) Nicholls, J. R. *Chem. Ind. London* **1934**, 53, 1077–1087.
- (4) Van Tassel, R. *Acta Crystallogr.* **1958**, 11, 745–746.
- (5) Fitzhugh, E. W.; Gettens, R. J. Calcilacite and Other Efflorescent Salts on Objects Stored in Wooden Museum Cases. In *Science and Archaeology*; Brill, R., Ed.; MIT Press: Cambridge, MA, 1971; pp 91–102.
- (6) Gibson, L. T.; Cooksey, B. G.; Littlejohn, D.; Linnow, K.; Steiger, M.; Tennent, N. H. *Stud. Conserv.* **2005**, 50, 284–294.
- (7) Linnow, K.; Halsberghe, L.; Steiger, M. *J. Cult. Herit.* **2007**, 8, 44–52.
- (8) Gibson, L. T.; Cooksey, B. G.; Littlejohn, D.; Tennent, N. H. *Anal. Chim. Acta* **1997**, 337, 151–164.
- (9) Linnow, K. *Salt Damage in Porous Materials*; University of Hamburg, Ph.D. Thesis, 2007.
- (10) Dinnebier, R. E.; Runčevski, T.; Fischer, A.; Eggert, G. *Inorg. Chem.* **2015**, 54, 2638–2642.
- (11) Runčevski, T.; Dinnebier, R. E.; Magdysyuk, O. V.; Pöllmann, H. *Acta Crystallogr., Sect. B* **2012**, 68, 493–500.
- (12) Ropret, P.; Madariaga, J. M. *J. Raman Spectrosc.* **2014**, 45, 985–992.
- (13) Robinet, L.; Eremin, K.; Cobo del Arco, B.; Gibson, L. T. *J. Raman Spectrosc.* **2004**, 35, 662–670.
- (14) Runčevski, T.; Wu, C.; Yu, H.; Yang, B.; Dinnebier, R. E. *J. Am. Ceram. Soc.* **2013**, 96, 3609–3616.
- (15) TOPAS 4.2; Bruker AXS Inc.: Madison, Wisconsin, USA, 2009.
- (16) Coelho, A. A. *J. Appl. Crystallogr.* **2003**, 36, 86–95.
- (17) Pawley, G. S. *J. Appl. Crystallogr.* **1981**, 14, 357–361.
- (18) Cheary, R. W.; Coelho, A. A.; Cline, J. P. *J. Res. Natl. Inst. Stand. Technol.* **2004**, 109, 1–25.
- (19) Oszlányi, G.; Suto, A. *Acta Crystallogr. A* **2004**, 60, 134–141.
- (20) Karle, J.; Hauptman, H. *Acta Crystallogr.* **1956**, 9, 635–651.
- (21) Andreev, Y. G.; MacGlashan, G. S.; Bruce, P. G. *Phys. Rev. B* **1997**, 55, 12011–12017.
- (22) Rietveld, H. M. *J. Appl. Crystallogr.* **1969**, 2, 65–71.
- (23) Macrae, C. F.; Bruno, I. J.; Chisholm, J. A.; Edgington, P. R.; McCabe, P.; Pidcock, E.; Rodriguez-Monge, L.; Taylor, R.; van de Streek, J.; Wood, P. A. *J. Appl. Crystallogr.* **2008**, 41, 466–470.
- (24) Runčevski, T.; Petruševski, G.; Makreski, P.; Ugarkovic, S.; Dinnebier, R. E. *Chem. Commun.* **2014**, 50, 6970–6972.
- (25) Bravais, A. *Études Cristallographiques*; Gauthier-Villars: Paris, 1866.
- (26) Friedel, G. *Bull. Soc. Franc. Mineral.* **1907**, 326.
- (27) Donnay, J. D. H.; Harker, D. *Am. Mineral.* **1937**, 22, 446–467.
- (28) Docherty, R.; Clydesdale, G.; Roberts, K. J.; Bennema, P. *J. Phys. D: Appl. Phys.* **1991**, 24, 89.
- (29) Ito, K.; Bernstein, H. J. *Can. J. Chem.* **1956**, 34, 170–178.
- (30) Waterland, M. R.; Stockwell, D.; Kelley, A. M. *J. Chem. Phys.* **2001**, 114, 6249–6259.
- (31) Schönemann, A.; Kutzke, H.; Lendl, B.; Eggert, G. IRUG 7, March 28–31, 2006, New York, NY; Infrared and Raman User's Group, 2006, pp 88–93; <http://irug.org/uploads/event/irug-7-2006.pdf> (January 30, 2015).
- (32) Trentelman, K.; Stodulski, L.; Scott, D.; Back, M.; Stock, S.; Strahan, D.; Drews, A. R.; O'Neill, A.; Weber, W. H.; Chen, A. E.; Garret, J. *Stud. Conserv.* **2002**, 47, 217–227.